Session 2A5
Computational Methods in Electromagnetics

Analysis of EM Scattering and Radiation Using Characteristic Basis Function Method with Plane Wave Spectrum Approach

X. F. Que and Z.-P. Nie
University of Electronic Science and Technology of China, China

Characteristic basis function method (CBFM) can be used to analyze the electromagnetic scattering and radiation properties of PEC object, especially for periodic structure. Characteristic basis functions (CBFs) are higher level expansion functions for unknown induced current, which can be considered as numerical basis functions for each block. The CBFM reduces the matrix size to a small and manageable level. The most CPU-intensive part in CBFM is to compute the matrix vector product. The couplings between all the discretized elements should be calculated and used twice, one for generating the CBFs and the other for constructing the system matrix, which is an intolerable procedure when dealing with electrically large object of arbitrary shape.

In this paper, the plane wave spectrum (PWS) approach is used to accelerate the matrix vector product. Only near-field interaction will be calculated directly. This method also realizes a saving in the memory requirement. Unlike FMM and MLFMA, no iterative methods are needed because a reduced matrix will be obtained, which is typically 3 orders of magnitude smaller for a moderate size problem when compared to the conventional MoM and can be solved by direct inversion.

We use the CBFM/PWS technique to analyze the large antenna arrays and scattering problems of arbitrary conducting objects. Numerical examples validate the accuracy and efficiency of this method.

REFERENCES

1. Prakash, V. V. S. and R. Mittra, "Characteristic basis function method: a new technique for fast solution of integral equations [J]," *Microwave and Optical Technology Letters*, Vol. 36, No. 2, 95–100, 2003.
2. Yeo, J. H., V. V. S. Prakash, and R. Mittra, "Efficient analysis of a class of microstrip antennas using the characteristic basis function method," *Microwave Optical Technology Letters*, Dec. 2003.
3. Song, J., C. C. Lu, and W. C. Chew, "Multilevel fast multipole algorithm for electromagnetic scattering by large complex objects [J]," *IEEE Trans.*, AP-45, 1488–1492, 1997.

The Structures of Fields of Standing Axisymmetric Spherical Electromagnetic Waves with High Localization of Intensity of Electrical and Magnetic Fields

M. V. Pavlova and Y. A. Zyuryukin
Saratov State Technical University, Russia

In the present work the mathematical simulation of standing axisymmetric spherical electromagnetic waves in isotropic medium is carried out. It was supposed, that at centre of a coordinate system a certain receiver of converging spherical waves is, and also the device, capable to realise phase shift of this received wave, and element, that emits this delayed wave as a wave, diverging from centre. The analytical expressions for components standing spherical $E-$ and $H-$ of waves, depending on a phase shift of diverging spherical wave concerning converging are obtained. The equations of lines of force taking a phase shift into account, which define electrical lines of force for $E-$wave and magnetic lines of force for $H-$wave, are obtained. The pictures of lines of force of fields of standing spherical electromagnetic waves, that define new variety of modes with high localization and strength of intensity of electrical and magnetic fields are calculated and constructed.

The Electromagnetic Effect of Different Sources on Pin-fin Heatsinks

S. B. Chiu and J. H. Chou
National Cheng Kung University, Taiwan

Due to the geometric features of heatsinks, the heatsinks may have adverse effects on electromagnetic radiation as the operating frequency of electronic devices increases to the gigahertz range. Different electromagnetic sources are often used in various practical applications. Thus the influence of electromagnetic interference (EMI) from different sources on heatsinks needs to be considered.

A finite difference time domain (FDTD) technique is used to investigate to the EM effect of different sources on pin-fin heatsinks. Seven fin configurations are investigated; namely, one without any fin, a metal block fin, and five pin fins with pin numbers of 2×2, 3×3, 4×4, 5×5, 6×6 respectively. Two types of excitation sources are studied, including a smooth compact pulse and a modulated Gaussian pulse with frequencies ranging from 0.8 GHz to 10 GHz.

The computational results show that at the low frequency of 0.8 GHz, for both types of excitation sources, only the heatsink with 6×6 pins exhibits obvious resonant phenomenon in electric fields. The difference lies in the extent of resonant levels. The resonant effect is larger for the case with modulated pulse source. At 4 GHz, the resonant behavior occurs at all fin configurations except the 3×3 pin-fin heatsink, irrespective of the difference in excitation sources. At this operating frequency, the resonant points and radiated magnitudes caused by the heatsinks for two sources are similar. At 10 GHz, multiple resonant points are observed. Furthermore, the resonant points move toward a distribution of high frequencies for the case of the smooth compact pulse excitation source. In contrast, the spectrum distribution resulted from the modulated Gaussian pulse source is concentrated mostly at discrete frequencies. In other words, the response due to different excitation source is insignificant at lower operation frequencies. But at higher operation frequencies, the difference in excitation sources can be significant and should be careful interpreted.

A Fast Solution of Combined Field Volume Integral Equation for EM Scattering

X. C. Nie, **N. Yuan**, **Y. B. Gan**, **and L. W. Li**
National University of Singapore, Singapore

The volume integral equation (VIE) approach is one of the most popular methods for electromagnetic scattering problems due to its flexibility in treating inhomogeneous objects. However, so far, VIE has been applied only to objects with non-magnetic materials (*i.e.*, $\mu=\mu_0$), and thus only the solution of the electric field volume integral equation (EFVIE) was considered. Materials with non-trivial permeability are often encountered in realistic applications, and hence, there exists a need to extend VIE to scatterers with arbitrary permeability (μ) and permittivity (ε).

In this paper, a combined field volume integral equation (CFVIE) is presented and solved for scattering from objects with arbitrary permittivity and permeability. Since the material has permeability (μ) that is different from the background medium, a magnetic volume current is required in addition to the electric volume current. This resulted in a coupled EFVIE and MFVIE (magnetic field volume integral equation), known as the combined field volume integral equation (CFVIE). The CFVIE is then solved using method of moments (MoM) to obtain the two unknown functions. However, as is well known, the traditional MoM cannot handle electrically large objects due to excessive memory requirement and computational complexity. To alleviate this problem, we need to leverage on recently developed fast algorithms, such as conjugate gradient fast Fourier transform (CG-FFT) method, multilevel fast multipole algorithm (MLFMA), adaptive integral method (AIM) and pre-corrected fast Fourier transform (P-FFT) method. However, all these algorithms have been restricted to FFVIE for purely dielectric objects so far. For CFVIE, the CG-FFT method is not applicable as the resultant matrix equation does not possess Toeplitz property. In contrast, the irregular-mesh-based P-FFT and AIM methods remain usable, although the extension is not trivial.

In this paper, we extended the P-FFT method to CFVIE to facilitate analysis of large inhomogeneous scatterers. The P-FFT method avoids the filling and storage of the usual coefficient square matrix. In the implementation of the P-FFT method, two sets of projection operators are constructed for the projections of the electric and magnetic sources, respectively. In addition, two sets of interpolation operators are also applied to the computation of vector/scalar potentials and the curl of vector potentials, respectively, in the support of the testing functions. The interpolation operators operate only on the Green's function, and thus are valid for any kind of basis functions. The resultant method has a memory requirement of O(N) and a computational complexity of O($N\log N$) respectively, where N is the number of unknowns. Due to the significant reduction in computational requirements as compared to the traditional MoM, the present method can analyze complex dielectric and magnetic objects of much larger sizes.

Broadband MLFMA for Electromagnetic Scattering by Dielectric Objects

H. Wallén, S. Järvenpää, P. Ylä-Oijala, and J. Sarvas
Helsinki University of Technology, Finland

In this talk we present a broadband algorithm for the electromagnetic scattering by a homogeneous dielectric object in the 3D space. For handling a large number of unknowns we use a broadband multilevel fast multipole algorithm (MLFMA).

In order to make the iterative solver for MLFMA to converge sufficiently fast, we use a well-conditioned Mueller surface integral equation formulation [1], which provides a broadband formulation for this field problem. One obtains this formulation by writing the EFIE and MFIE equations at both sides (1 and 2) of the surface of the object for the unknowns $\mathbf{J} = \mathbf{n} \times \mathbf{H}$ and $\mathbf{M} = -\mathbf{n} \times \mathbf{E}$, $\mathbf{n}$ being the outer unit normal of the surface, and then combining the equations as

$$-\alpha_1(MFIE_1) + \alpha_2(MFIE_2) \text{ and } \beta_1(EFIE_1) - \beta_2(EFIE_2)$$

with multipliers $\alpha_j = 2\mu_j/(\mu_1 + \mu_2)$, $\beta_j = 2\epsilon_j/(\epsilon_1 + \epsilon_2)$, $j = 1, 2$.

In our broadband MLFMA [2] we use the traditional MLFMA for levels with division cube sidelength $\geq \lambda/2$, λ being the wavelength, and for levels with smaller cube sidelengths we use an MLFMA based on the spectral representation of the Green's function. In the Mueller formulation the exterior and the interior of the object need MLFMA procedures of their own because they have different wave numbers.

In each iteration step for the matrix-vector product, we need to compute the fields $\mathbf{E^{sc}}$ and $\mathbf{H^{sc}}$ due to the given surface currents $\mathbf{J}$ and $\mathbf{M}$. We get the components of the matrix-vector product by adding these currents, multiplied by suitable constants, and by taking inner products with the relevant testing functions.

The outgoing fields are presented by their radiation patterns. For translating the outgoing fields $\mathbf{E^{sc}}$ and $\mathbf{H^{sc}}$ from a division cube Q to incoming plane-wave expansions in a non-nearby cube we only need to store the radiation and incoming wave patterns of $\mathbf{E^{sc}}$, because both $\mathbf{E^{sc}}$ and$\mathbf{H^{sc}}$ are obtained directly from them. These patterns are computed easily from $\mathbf{J}$ and $\mathbf{M}$ in Q, and they are stored in three Cartesian components to make the interpolation and anterpolation procedures work in an efficient manner.

We demontrate the resulting broadband MLFMA algorithm by a numerical example, where the bistatic RCS is computed for dielectric spheres with diameters varying from $\lambda/100$ to 3λ and using several levels in MLFMA. A good agreement with the Mie-series results are obtained with reasonable numbers of iterations.

REFERENCES

1. Ylä-Oijala, P. and M. Taskinen, *IEEE Trans. Antennas Propagat.*, Vol. 53, No. 10, 3316–3323, Oct. 2005.
2. Wallén, H. and J. Sarvas, *Progress in Electromagnetics Research*, Vol. 55, 47–78, 2005.

Arbitrary Lagrangian Eulerian Electromechanics in 3D

R. Rieben, B. Wallin, and D. White
Lawrence Livermore National Laboratory, USA

Abstract—We present results from an effort to couple the equations of electromagnetic diffusion with the equations of arbitrary Lagrangian-Eulerian (ALE) hydrodynamics. The electromagnetic diffusion equations are discretized using a novel mixed finite element method coupled with a generalized Crank-Nicholson time differencing scheme. At each discrete time step, electromagnetic force and heat terms are calculated and coupled to the hydrodynamic equations in an operator split approach. We present preliminary results from a fully coupled electromechanical simulation as well as results concerning advection techniques for electromagnetic quantities.

1. Introduction

We are interested in the simulation of electromechanical devices and magnetohydrodynamic events in three dimensions. Our primary goal is a numerical method that solves, in a self-consistent manner, the equations of electromagnetics (primarily statics and diffusion), heat transfer (primarily conduction), and non-linear mechanics (elastic-plastic deformation, and contact with friction). In this paper, we focus on the numerical discretization of electromagnetic diffusion in an arbitrary Lagrangian-Eulerian (ALE) fashion for the purposes of computing $\vec{J}\times\vec{B}$ forces for mechanical (or hydrodynamic) calculations and $\vec{J}\cdot\vec{E}$ Joule heating terms for thermal calculations.

The equations of electromagnetic diffusion can be derived from the full wave Maxwell equations by making the good conductor approximation (i. e., ignoring displacement current), which is standard practice in magnetohydro- dynamic (MHD) formulations. For conducting materials moving with a velocity $\vec{v}$ with respect to a fixed Eulerian (or laboratory) frame, we can derive the so called dynamo equation (also known as the hydromagnetic equation) in terms of magnetic flux density

$$\frac{\partial \vec{B}}{\partial t} = -\vec{\nabla} \times (\frac{1}{\sigma}\vec{\nabla} \times \frac{1}{\mu}\vec{B}) + \vec{\nabla} \times (\vec{v} \times \vec{B}) \tag{1}$$

In the Eulerian description the velocity $\vec{v}$ is a function of time t and position $\vec{x}$. In the *Lagrangian* (or material) description (which we will designate with a "prime" symbol), the flow is described by following the position $\vec{x}(\vec{x}', t)$ of the material point that started at position $\vec{x}'$ at $t = 0$. In functional form, we have

$$\vec{x}' = \vec{x}'(\vec{x}, t); \quad \vec{x} = \vec{x}(\vec{x}', t)$$

To convert between the two representations, we define the Jacobian matrix as

$$J_{i,j} = \frac{\partial x'_j}{\partial x_i} \tag{2}$$

As shown in [1], the following quantities are invariant with respect to the Lagrangian-Eulerian representations

$$\begin{array}{rcl} \textit{Lagrangian} & & \textit{Eulerian} \\ \vec{E}' \cdot d\vec{x}' & = & (\vec{E} + \vec{v} \times \vec{B}) \cdot d\vec{x} \\ \vec{B}' \cdot d\vec{a}' & = & \vec{B} \cdot d\vec{a} \end{array} \tag{3}$$

It is well known that differential arc length and surface area elements transform according to

$$d\vec{x}' = J^T d\vec{x} \tag{4}$$

$$d\vec{a}' = |J|J^{-1} d\vec{a} \tag{5}$$

As a consequence, the electric field intensities and magnetic flux densities must transform inversely to maintain the invariance property of (3)

$$\vec{E}' = J^{-1}(\vec{E} + \vec{v} \times \vec{B}) \tag{6}$$

$$\vec{B}' = \frac{1}{|J|} J^T \vec{B} \tag{7}$$

The dynamo equation in the Lagrangian frame is therefore

$$\frac{d\vec{B}'}{dt} = -\vec{\nabla}' \times (\frac{1}{\sigma}\vec{\nabla}' \times \frac{1}{\mu}\vec{B}') \tag{8}$$

In a typical ALE hydrodynamic calculation, an *operator split* method is employed where all calculations are performed on a Lagrangian mesh (i. e., a mesh that moves with the materials). When the Lagrange motion of the mesh causes significant mesh distortion, that distortion is corrected with an equipotential relaxation of the mesh, followed by a 2nd order monotonic remap of mesh quantities. This remap is equivalent to an advection of material through the mesh. In our proposed ALE formulation of MHD, we will employ an operator-split method with three distinct steps:

- *Electromagnetic Diffusion*–Solve the dynamo equation in the Lagrangian frame at one discrete time step for fixed materials.
- *Lagrangian Motion*–Move mesh nodes according to $\vec{J}' \times \vec{B}'$ forces assuming a $\frac{d\vec{B}'}{dt} = 0$ "frozen flux" condition.
- *Eulerian Advection*–Only required if mesh is relaxed, advect (or transport) magnetic (vector potential) flux quantities to new mesh.

Note that the second step (effectively "dragging" the electromagnetic quantities along with the mesh during Lagrangian motion) will only work if our discretization of the electromagnetic quantities satisfies the invariance relation of (3) (see also [2]). In the Eulerian advection step of the calculation, the computed electromagnetic degrees of freedom must be "remapped" or "advected" in a way which preserves a discrete divergence-free property of the magnetic flux density with minimal magnetic energy loss.

2. Numerical Formulation

The divergence-free (or solenoidal) nature of the magnetic flux density, $\vec{\nabla}' \cdot \vec{B}' = 0$, implies that $\vec{B}' = \vec{\nabla}' \times \vec{A}'$ where $\vec{A}'$ is a magnetic vector potential. This in turn implies that the electric field in the Lagrangian frame is given by $\vec{E}' = -\vec{\nabla}'\phi' - \frac{\partial}{\partial t}\vec{A}'$, where ϕ' is an electric scalar potential. Using the gauge condition $\vec{\nabla}' \cdot \sigma\vec{A}' = 0$, we can reformulate the dynamo equation (8) in terms of potentials as

$$\vec{\nabla}' \cdot \sigma\vec{\nabla}'\phi' = 0 \tag{9}$$

$$\sigma\frac{d\vec{A}'}{dt} = -\vec{\nabla}' \times \frac{1}{\mu}\vec{\nabla}' \times \vec{A}' - \sigma\vec{\nabla}'\phi' \tag{10}$$

Note that this formulation has an additional elliptic PDE (9) to solve for the scalar potential. A key advantage of this formulation is that voltage, which is often the only known quantity for electromechanical engineering applications, appears explicitly in the equations as an essential boundary condition for the elliptic solution of (9). To compute force and heat terms, we define the *secondary variables* in terms of the potentials as

$$\vec{B}' = \vec{\nabla}' \times \vec{A}' \tag{11}$$

$$\vec{J}' = \sigma\vec{E}' = -\vec{\nabla}'\phi' - \frac{d}{dt}\vec{A}' \tag{12}$$

Finally, there are divergence constraints on both the primary and secondary fields, namely

$$\vec{\nabla}' \cdot \sigma\vec{A}' = 0 \tag{13}$$

$$\vec{\nabla}' \cdot \vec{B}' = 0 \tag{14}$$

To discretize the potential formulation in the Lagrangian frame, we apply the mixed finite element methods (FEM) of [3] which are based on the properties of differential forms and have been shown to preserve discrete divergence-free properties and to maintain accuracy in secondary variables (e.g., $\vec{J}$ and $\vec{B}$) even when computed from potentials. Most importantly, the discrete vector fields transform identically to (6) and (7), thereby preserving the invariance property of (3).

In our proposed ALE formulation the scalar potential will be discretized on mesh nodes (i. e., a discrete 0-form field), the vector potential will be discretized on mesh edges (i. e., a discrete 1-form field) and the secondary variables $\vec{B}$ and $\vec{J}$ will be discretized on mesh faces (i. e., discrete 2-form fields) as follows

$$\phi' \approx \sum_{i=1}^{n} v_i W_i^0 \tag{15}$$

$$\vec{A}' \approx \sum_{i=1}^{n} a_i \vec{W}_i^1 \tag{16}$$

$$\vec{B}' \approx \sum_{i=1}^{n} b_i \vec{W}_i^2 \tag{17}$$

$$\vec{J}' \approx \sum_{i=1}^{n} j_i \vec{W}_i^2 \tag{18}$$

where W^l denotes a discrete l-form basis function. In [3], various mass, stiffness, derivative and discrete Hodge matrices are defined. Given these matrices, the fully discrete form of the potential diffusion equation is given in [3] by applying a Generalized Crank-Nicholson method to obtain

$$\mathbf{S}^0 \mathbf{v}_{n+\alpha} = \mathbf{f}^0_{n+\alpha} \tag{19}$$

$$(\mathbf{M}^1(\sigma) + \alpha \Delta t \mathbf{S}^1(\mu^{-1}))\mathbf{a}_{n+1} = (\mathbf{M}^1(\sigma) - (1-\alpha)\Delta t\ \mathbf{S}^1(\mu^{-1}))a_n - \Delta t \mathbf{D}^{01}\mathbf{v}_{n+\alpha} \tag{20}$$

where $\alpha \in [0.1]$ is weighting parameter which determines the type of integration such that

$$\alpha = \begin{cases} 0 & \text{Explicit, 1st Order Accurate Forward Euler} \\ 1/2 & \text{Implicit, 2nd Order Accurate Crank Nicholson} \\ 1 & \text{Implicit, 1st Order Accurate Backward Euler} \end{cases}$$

Once the values for the primary potentials have been solved for, the discrete secondary fields can be computed as

$$\mathbf{e}_{n+\alpha} = -\mathbf{K}^{01}\mathbf{v}_{n+\alpha} - 1/\Delta t(\mathbf{a}_{n+1} - \mathbf{a}_n) \tag{21}$$

$$\mathbf{b}_{n+1} = \mathbf{K}^{12}\mathbf{a}_{n+1} \tag{22}$$

$$\mathbf{M}^2(\sigma^{-1})\mathbf{j}_{n+\alpha} = \mathbf{H}^{12}\mathbf{e}_{n+\alpha} \tag{23}$$

These terms are used to compute $\vec{J}' \times \vec{B}'$ forces which will accelerate the mesh nodes during the Lagrangian motion step. The discrete divergence constraints are given by

$$(\mathbf{D}^{01}(\sigma))^T\mathbf{a} = 0 \tag{24}$$

$$(\mathbf{D}^{01}(\sigma))^T\mathbf{e} = 0 \tag{25}$$

$$\mathbf{K}^{23}\mathbf{b} = 0 \tag{26}$$

and as shown in [3], these constraints are implicitly satisfied for all time, assuming the initial conditions and the source terms are divergence free.

To demonstrate a fully coupled Lagrangian calculation, we consider a numerical experiment in which a 5 KV capacitor bank is discharged into a can shaped aluminum structure (see Fig. 1). The voltage through the can (effectively an inductive and resistive load) is computed via a simple SPICE model. The resulting voltage vs. time profile is then used as an essential boundary condition for the discrete scalar potential solve of (19) which

drives the problem. An essential boundary condition of the form $\hat{n} \times \vec{A}' = 0$ is applied to the front side of the mesh while the remainder of the surface is subject to the natural boundary condition $\hat{n} \times \frac{1}{\mu}\vec{\nabla}' \times A' = 0$. A peak current of roughly 0.8 MA is generated in the can, creating a $\vec{J}' \times \vec{B}'$ force which causes the can to initially compresses (or implode). However, the force is not strong enough to cause the aluminum can to yield, and so the can effectively rings over time in an elastic response as shown in Figs. 1 and 2.

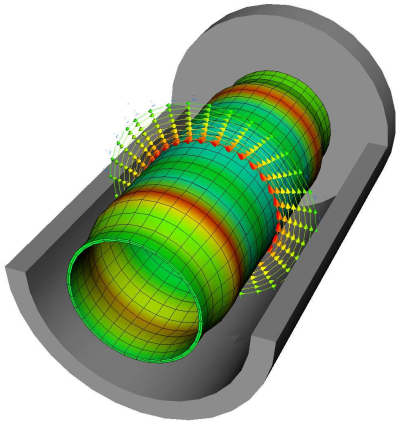

Figure 1: Snapshot of the fully coupled electromechanical simulation. In this image the aluminum can is elastically expanding after initially being compressed. The displacement has been exaggerated by a factor of 300 for visual clarity.

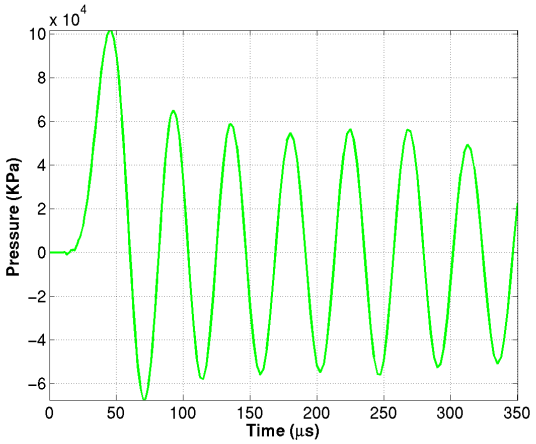

Figure 2: Measured pressure response in the aluminum can due to an electromagnetic force.

3. Constrained Transport Methods on Unstructured Grids

During the optional Eulerian advection phase of our operator split method, the computed electromagnetic values must be remapped (or advected). Remapping refers to the process of updating the representation of the field given a new grid. We consider only new grids which are "nearby" in the sense that only small perturbations of the grid are allowed (i. e., the mesh nodes should not travel farther than one mesh element in any one time step). This is known as the continuous remap approximation (CRA).

We propose to use the so called *constrained transport* method originally developed by [4] and later expanded by [5]. Suppose we have calculated the magnetic flux density $\vec{B}'$ in a Lagrangian time step via (22), we then have a local element representation of $\vec{B}'$

$$\vec{B}^{old} \approx \sum_{i=1}^{n} b_i^{old} \vec{W}_i^{2,old} \tag{27}$$

The degrees of freedom (DOF) b_i^{old} in this expansion carry the units of magnetic *flux*. For the special case of lowest order ($p = 1$) basis functions (i. e., six DOF per element), this implies that we know the magnetic flux through every face in the Lagrangian mesh (or the "*old*" mesh). Now in a standard ALE step, the old mesh is relaxed under the CRA to a *new* mesh. Therefore, our goal is to compute *new* values of the magnetic flux b_i^{new} which will allow us to represent the magnetic flux density on the new mesh. For the special case of lowest order (p = 1) basis functions, the discrete divergence free property is simply a statement that the 6 fluxes in the face sum to zero. The goal of *constrained* transport is to preserve this property on the new mesh.

For unstructured hexahedral grids, we can update the magnetic flux (or "vector potential flux" $\vec{A} \cdot d\vec{x}$) by effectively solving Faraday's law for a moving conductor (equivalent to magnetic transport under the "frozen-flux" condition)

$$\Phi^{new} \approx \Phi^{old} - \oint_C (\vec{u} \times \vec{B}) \cdot d\vec{l} \tag{28}$$

where $\vec{u}$ is the mesh displacement. Our goal now is to apply (28) in an algorithmic fashion to update the fluxes on the faces of a new mesh. A schematic representation of this process is shown in Fig. 3. It is clear from

the depiction of Fig. 3 that we can approximate the flux through a new face given the flux through the old face and a "measurement" of the time rate of change of flux (an effective voltage) along the closed circuit path C depicted in green. For a given face in the new mesh, the algorithm of (28) can be used to update the edge flux contributions

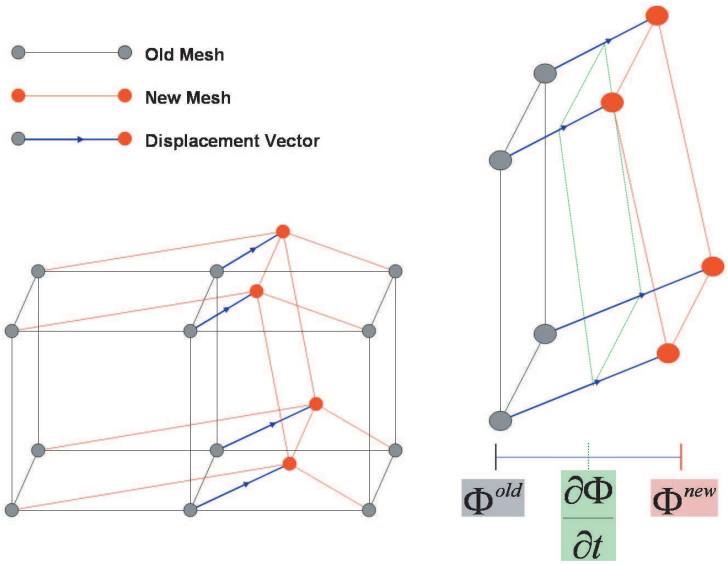

Figure 3: Schematic diagram depicting the relationship between magnetic flux through "old" and "new" mesh faces and the most accurate location for "measuring" the update EMF.

$\vec{A} \cdot dx$ for each edge in the face (thereby updating the vector potential) or the total magnetic flux $\vec{B} \cdot d\vec{a}$ through the face. By construction, the new flux values will sum to zero, provided the old fluxes do so as well. In order for this algorithm to work, $\vec{B}$ must be evaluated at the displacement vector midpoints for the discrete path integral; however, this is problematic for faced based representations of $\vec{B}$, since they are by construction, discontinuous along element edges. To overcome this, a "smooth" $\vec{B}$ field must be patch recovered using a continuous vector nodal approximation.

4. Conclusions

We have presented and discussed an operator split approach for solving the coupled equations of electromechanics and magnetohydrodynamics using the novel mixed finite element methods of [3] to discretize the equations of electromagnetic diffusion. We have presented preliminary results for a fully coupled Lagrangian calculation and have discussed methods for advecting magnetic flux for ALE calculations.

Acknowledge

This work was performed under the auspices of the U.S. Department of Energy by the University of California, Lawrence Livermore National Laboratory under contract No. W-7405-Eng-48, UCRL-ABS-215152.

REFERENCES

1. Lax, M. and D. F. Nelson., "Maxwell equations in material form," *Phys. Rev. B*, Vol. 13, No. 14, 1777–1784, 1975.
2. Hu, P. J., A. Robinson, and R. Tuminaro., "Towards robust z-pinch simulations: discretization and fast solvers for magnetic diffusion in heterogenous conductors," *Electronic Trans. Num. Analysis*, Vol. 15, 186–210, 2003.
3. Rieben, R. and D. White., "Verification of high-order mixed fem solution of transient magnetic diffusion problems.," *IEEE Trans. Mag.*, article in press, October 2005.
4. Evans, C. R. and J. F. Hawley, "Simulation of magnetohydrodynamic flows: a constrained transport method," *The Astrophysical Journal*, Vol. 332, 659–677, 1988.
5. Bochev, P. and M. Shaskov., "Constrained interpolation (remap) of divergence-free fields," *Comput. Methods Appl. Mech. Engrg.*, Vol. 194, 511–530, 2005.

Hybrid Numerical Simulation of Micro Electro Mechanical Systems

M. Greiff, U. B. Bala, and W. Mathis
University of Hanover, Germany

Abstract—In this paper a hybrid numerical approach for the simulation of micro electro mechanical systems (MEMS) is presented. A simulation model that takes into account the mechanical and the electrical effects is developed. The model is applied to an electrostatic force microscope (EFM) and simulation results are presented.

1. Introduction

Although micro electro mechanical systems (MEMS) already exist for many applications, their calculation is still difficult since in order to obtain accurate results, ofter times multi scale aspects have to be included. Furthermore the coupled mechanical and electrical behavior has to be taken into account. In our work this is achieved by dividing the model into a mechanical and an electrical part. The interaction between them is shown in Fig. 1 and can conveniently be realized by using a staggered simulation approach. The electric forces are calculated by the electrical part and passed to the mechanical part which uses them as input for the calculation of the mechanical deflection. In order to apply this approach to a two dimensional model of an electrostatic force microscope (EFM) (Fig. 2) both parts have to be defined. Therefore the components and the principle of an EFM will be explained in the following. An EFM is used to scan surfaces holding an electric potential or a charge distribution [1–3]. During the scanning process the tip at the end of the cantilever is run over the sample. The forces acting on the cantilever and the tip are determined by the electrostatic field and calculated by the electrostatic part of the model. The mechanical behavior of the cantilever is modelled using a beam model while for the region near the tip the finite element method (FEM) is used. A more detailed description of the electrical part will be given in the following.

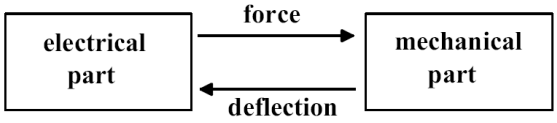

Figure 1: Mechanical and electrical part.

2. Formulation of the Problem

The energy-related functional in the electrostatic calculation domain Ω (Fig. 2) can be written as

$$W = \int_{\Omega} (\nabla u)^2 d\Omega \qquad u \in H_D^1(\Omega) : \{u \in H^1 | u_{|\Gamma_D} = u_0\} \tag{1}$$

where $u(a_1, a_2, \ldots, a_m, x, y)$ is an approximation of the potential $u(x, y)$. It is well known that the solution of

$$\frac{\partial W}{\partial a_i} = 2 \int_{\Omega} \nabla u \frac{\partial \nabla u}{\partial a_i} d\Omega = 0 \tag{2}$$

yields an approximative solution for the Laplace equation in Ω. In order to solve (2) numerically we shall take a closer look at the requirements in the different parts of the calculation domain Ω. Since most of the interaction between probe and sample happens at the bottom of the tip, accurate calculation results are important in this region. Therefore a numerical method which is able to deal with the high field values near the tip is required. For this reason the method of fundamental solutions (MFS) is applied in region Ω_M (Fig. 3). At a larger distance from the tip (region Ω_F) lower field values are expected, but possible nonlinearities and charge distributions in the sample require a versatile numerical method such as the finite element method (FEM). Because of the large difference in size of tip and cantilever length, FEM cannot conveniently be applied in the whole rest of the calculation domain. Therefore the boundary element method (BEM) that only requires a mesh on the boundary is used in region Ω_B.

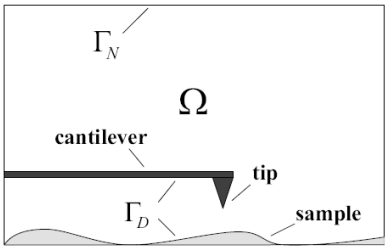

Figure 2: Electrostatic force microscope and calculation domain.

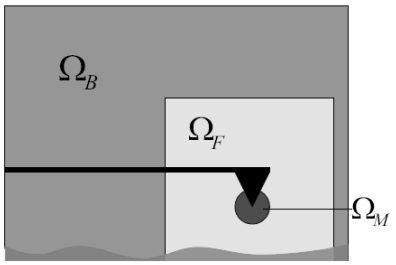

Figure 3: Divided calculation domain.

The solutions in the circular region Ω_M of radius R can be expanded into

$$u(\rho,\phi) = V_0 + \sum_{i=1}^{m} c_i \left(\frac{\rho}{R}\right)^{\frac{i\pi}{\beta}} \sin(\frac{i\pi\phi}{\beta}), \quad (\rho,\phi) \in \Omega_M \tag{3}$$

where V_0 is the electric potential and β is the outer opening angle of the tip [4]. For the choice of R and the position and the number of coupling points, the overlapping area of Ω_M and Ω_F must be small. Furthermore it must be considered that (3) is a good approximation of the potential only near the tip.

In region Ω_F linear FEM

$$u(x,y) = \sum_{j=1}^{n} u_j \psi_j(x,y), \quad (x,y) \in \Omega_F \tag{4}$$

is applied [5]. The solutions of both regions [6] are coupled by

$$u_c = V_0 + \sum_{i=1}^{m} c_i \sin(\frac{i\pi\phi_c}{\beta}). \tag{5}$$

Replacing the coupling node potentials in (4) by (5) and using the resulting potential functions in (2) leads to

$$\begin{pmatrix} M & B^T \\ B & F \end{pmatrix} \begin{pmatrix} c \\ u_F \end{pmatrix} = \begin{pmatrix} b_M \\ b_F \end{pmatrix} \tag{6}$$

where $\mathbf{M}$ is the matrix resulting from the MFS that is defined by

$$M_{ij} = 2 \sum_{k\in n_c} \sum_{m\in n_c} \sin\left(\frac{i\pi}{\beta}\phi_k\right) \sin\left(\frac{j\pi}{\beta}\phi_m\right) \int_{\Omega_F} \nabla(\psi_k)\nabla(\psi_m) d\Omega + \begin{cases} i\pi, & i=j \\ 0, & \text{otherwise,} \end{cases} \tag{7}$$

$$F_{ij} = 2 \int_{\Omega_F} \nabla\psi_i \nabla\psi_j d\Omega \tag{8}$$

is the FEM stiffness matrix,

$$B_{ij} = 2 \sum_{k\in n_c} \sin\left(\frac{j\pi}{\beta}\right) \int_{\Omega_F} \nabla\psi_i \nabla\psi_k d\Omega \tag{9}$$

is the FEM-MFS coupling matrix,

$$b_{Mi} = -2V_0 \sum_{k\in n_c} \sum_{m\in n_c} \sin\left(\frac{i\pi}{\beta}\right) \int_{\Omega_F} \nabla\psi_k \nabla\psi_m d\Omega \tag{10}$$

is the MFS right hand side and

$$b_{Fi} = -2V_0 \sum_{k\in n_c} \int_{\Omega_F} \nabla\psi_i \nabla\psi_k d\Omega_F - 2 \sum_{j\in n_D} \phi_j \int_{\Omega_F} \nabla\psi_i \nabla\psi_j d\Omega \tag{11}$$

is the right hand side resulting from the variation of the FEM potentials. Here n_c stands for the coupling nodes and n_D are the Dirichlet boundary conditions. The matrix F can be written as

$$\mathbf{F} = \begin{pmatrix} F_{NN} & F_{CN}^T \\ F_{CN} & F_{CC} \end{pmatrix} \tag{12}$$

where F_{NN} includes only the interaction between the nodes inside the FEM domain, F_{CC} stands for the interaction inside the coupling interface while the interaction of coupling interface and FEM domain is described by F_{CN}.

On the FEM-BEM transmission interface $\Gamma_T = \Gamma_B \cap \Gamma_F$: $u_B = u_F$ and $\frac{\partial u_B}{\partial n} + \frac{\partial u_F}{\partial n} = 0$. Using the Gauss theorem on $\Omega_{FM} = \Omega_F \cup \Omega_M$ one obtains [5]

$$\int_{\Gamma_F} \frac{\partial u_{FM}}{\partial n} v \; d\Gamma = \int_{\Omega_{FM}} \operatorname{div}(\nabla u_{FM} \cdot v) \; d\Omega = \int_{\Omega_{FM}} \Delta u_{FM} \cdot v \; d\Omega + \int_{\Omega_{FM}} \nabla u_{FM} \cdot \nabla v \; d\Omega \tag{13}$$

i. e., for all $v \in H^1_{D,0}(\Omega_{FM}) := \{v \in H^1(\Omega_{FM}) : v|_{\Gamma_D \cap \Gamma_F} = 0\}$

$$a(u_{FM}, v) := \int_{\Omega_{FM}} \nabla u_{FM} \cdot \nabla v \; d\Omega = \int_{\Omega_{FM}} f \cdot v \; d\Omega + \int_{\Gamma_F} \frac{\partial u_{FM}}{\partial n} v \; d\Gamma =: (f, v)_{\Omega_{FM}} + \langle \frac{\partial u_{FM}}{\partial n}, v \rangle_{\Gamma_F} \tag{14}$$

where u_{FM} includes u_F and c. The representation formula of the Laplace equation for the solution of u_B inside Ω_B

$$u_B(x) = \int_{\Gamma_B} \{\frac{\partial}{\partial n(y)} G(x,y) u_B(y) - G(x,y) \frac{\partial u_B}{\partial n(y)}\} d\Gamma, \quad x \in \Omega_B \tag{15}$$

with the fundamental solution of the Laplacian given by

$$G(x,y) = -\frac{1}{2\pi} \log |x - y|. \tag{16}$$

If one computes the Cauchy data [7] u_B and $\partial u_B / \partial n$ of $u_B(x)$, one will get two boundary integral equations on $\partial\Omega_B$,

$$V \frac{\partial u_B}{\partial n} = (I + K) u_B \tag{17}$$

$$W u_B = (I - K') \frac{\partial u_B}{\partial n} \tag{18}$$

where the boundary integral operators are defined as

$$V\psi(x) := 2 \int_{\Gamma_B} G(x,y) \psi(y) d\Gamma_y, \quad K\psi(x) := 2 \int_{\Gamma_B} \frac{\partial}{\partial n_y} G(x,y) \psi(y) d\Gamma_y, \quad x \in \Gamma_B \tag{19}$$

$$K'\psi(x) := 2 \frac{\partial}{\partial n_x} \int_{\Gamma_B} G(x,y) \psi(y) d\Gamma_y, \quad W\psi(x) := -2 \frac{\partial}{\partial n_x} \int_{\Gamma_B} \frac{\partial}{\partial n_y} G(x,y) \psi(y) d\Gamma_y, \quad x \in \Gamma_B \tag{20}$$

where the single layer potential V and the hypersingular operator W are symmetric and the double layer potential K has the dual K' [8].

Using (18) one can eliminate $\partial u_B / \partial n$ with (17). This leads to

$$W u_B = (I - K') \frac{\partial u_B}{\partial n} = 2 \frac{\partial u_B}{\partial n} - (I + K') \frac{\partial u_B}{\partial n} = 2 \frac{\partial u_B}{\partial n} - (I + K') V^{-1} (I + K) u_B \tag{21}$$

with the Poincaré-Steklov-Operator S applied to u_B

$$S u_B := (W + (I + K') V^{-1} (I + K)) u_B = 2 \frac{\partial u_B}{\partial n} \tag{22}$$

which can be used for symmetric coupling. In variational form for all $w \in \tilde{H}^{1/2} := \{w \in H^{1/2}(\Gamma_B) : w|_{\Gamma_D \cap \Gamma_B} = 0\}$ holds

$$\langle S u_B, w \rangle_{\Gamma_B} = 2 \langle \frac{\partial u_B}{\partial n}, w \rangle_{\Gamma_B}. \tag{23}$$

With (14) and (23) one can obtain the variational formulation

$$2a(u_{FM}, v) + \langle S u_B, v \rangle_{\Gamma_T} = 2(f, v)_{\Omega_{FM}} + 2\langle t_0, v \rangle_{\Gamma_N \cap \Gamma_F} \tag{24}$$

$$\langle S u_B, w \rangle_{\Gamma_B \cap \Gamma_N} = 2\langle t_0, w \rangle \tag{25}$$

for all $(w, v) \in \tilde{H}^{1/2} \times H^1_{D,0}(\Omega_F)$ with f being the charge distribution inside Ω_F and t_0 are the Neumann boundary conditions.

The Poincaré-Steklov-Operator S cannot discretize directly because the inverse single layer potential V cannot be descritized in the usual way. For this reason without Poincaré-Steklov-Operator the problem can be rewritten as saddle point formulation. The saddle point formulation of the problem for all $(w, v, \psi) \in \tilde{H}^{1/2} \times H^1_{D,0}(\Omega_{FM}) \times \tilde{H}^{-1/2}(\Gamma_B)$

$$2a(u_{FM}, v) + \langle W u_B, v\rangle_{\Gamma_T} + \langle (I + K')\varphi, v\rangle_{\Gamma_T} = 2(f, v)_{\Omega_{FM}} + 2\langle t_0, v\rangle_{\Gamma_N \cap \Gamma_F} \tag{26}$$

$$\langle W u_B, w\rangle_{\Gamma_B \cap \Gamma_N} + \langle (I + K')\varphi, w\rangle_{\Gamma_B \cap \Gamma_N} = 2\langle t_0, w\rangle_{\Gamma_B \cap \Gamma_N} \tag{27}$$

$$\langle (I + K) u_B, \psi\rangle_{\Gamma_B} - \langle V\varphi, \psi\rangle_{\Gamma_B} = 0 \tag{28}$$

If the bases are introduced as $\mathrm{span}\{v_1, \ldots\ldots, v_F\} = X_F$, $\mathrm{span}\{w_1, \ldots\ldots, w_F\} = X_B$ and $\mathrm{span}\{\psi_1, \ldots\ldots, \psi_F\} = Y_B$, the basis functions of X_F and X_B are supposed to be ordered such that

$$\mathrm{span}\{v_1, \ldots\ldots, v_F\} = X_F \cap H^1_{D,0}(\Omega_F)$$

$$\mathrm{span}\{w_1, \ldots\ldots, w_B\} = X_B \cap H^{1/2}(\Gamma_B).$$

If the coefficients of u_{FM} and u_B are denoted by u and the coefficients of φ are denoted by φ again then this system is equivalent to the original differential equation that can be used for descritization. This system corresponds to a matrix formulation which can be written as

$$\begin{pmatrix} M & B^T & 0 & 0 & 0 \\ B & F_{NN} & F_{NC} & 0 & 0 \\ 0 & F_{CN} & F_{CC} + W_{CC} & W_{CN} & (K^T + I)_C \\ 0 & 0 & W_{NC} & W_{NN} & (K^T + I)_N \\ 0 & 0 & (K + I)_C & (K + I)_N & -V \end{pmatrix} \begin{pmatrix} u_m \\ u_F \\ u_T \\ u_B \\ \varphi \end{pmatrix} = \begin{pmatrix} b_m \\ b_F \\ b_\Gamma \\ b_B \\ b_\varphi \end{pmatrix} \tag{29}$$

where the subscript C means contribution from the coupling nodes and N means contribution from the noncoupling nodes. Finally the blocks W, V, $K + I$, and $K^T + I$ provide the coupling between the two ansatz spaces X_F and X_B. Here u_m are the MFS coefficients, u_F and u_B are the nodal potentials inside the FE domain and on the boundary of the BE domain respectively, u_T are the nodal potentials on the FE-BE coupling interface and φ are the normal components of the electric field distribution on the boundary of the BE domain. The vector b includes the corresponding boundary conditions. As the matrix in (29) is not positive definite, a specific algorithm such as the MINRES algorithm is required for the solution.

Since the scanning process of an EFM is dynamic, the FEM mesh in Ω_F has to be changed during the calculation which is achieved by using the arbitrary Lagrangian Eulerian method (ALE) [9]. The mesh is modeled as a massless elastic which is deformed by the changing position of the cantilever and the sample (Fig. 4).

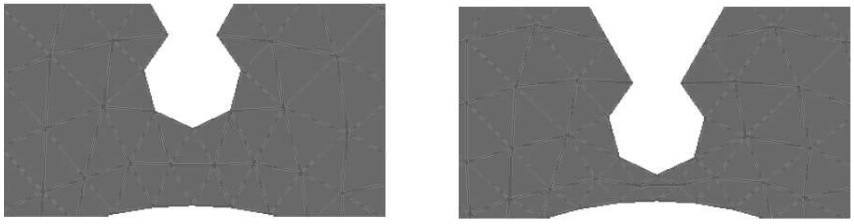

Figure 4: ALE mesh deformation.

The result of a typical simulation can be seen in Fig. 6 and Fig. 7. As expected a high value of the electric field occurs at the tip. Since the coupling condition of MFS and FEM only includes the potential values (5), the electric field is not continuous on the interface. This indicates that FEM simulation results near the tip can be improved by using the coupled FEM-MFS approach presented here. A smoother transition of the electric field can be obtained by using a combination of FEM and MFS ansatz functions in region Ω_M. Fig. 5 shows the simulated potential between tip and sample obtained by using FEM and the hybrid simulation approach ($R = 1$, 2).

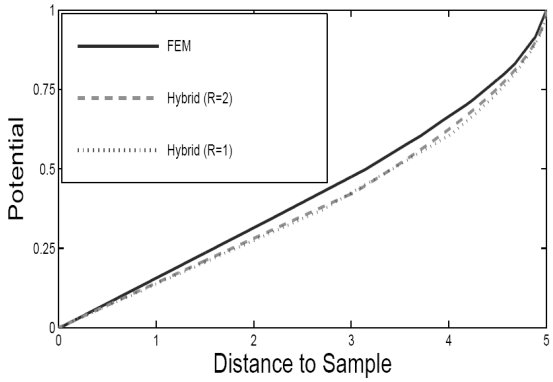

Figure 5: Comparison FEM/Hybrid Simulation.

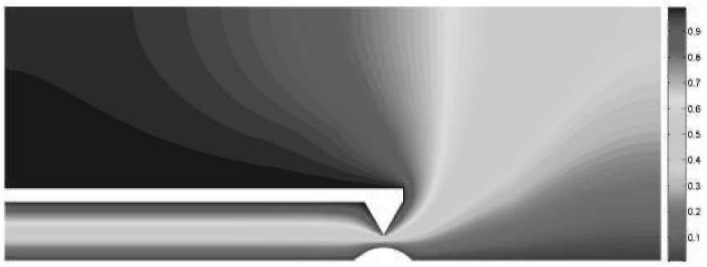

Figure 6: Simulated electrostatic potential.

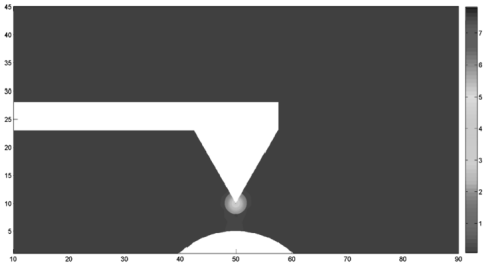

Figure 7: Simulated electrostatic field.

3. Conclusion

A hybrid numerical approach for the simulation of micro electro mechanical systems (MEMS) has been presented and applied to an electrostatic force microscope. In order to fulfill the special requirements in the different simulation regions an approach that combines FEM BEM and MFS was used to calculate the electrostatic field. ALE was applied to fit the FEM mesh to the changing boundaries. The results show the expected field distribution.

Acknowledgment

The authors would like to thank T. Helmich and Prof. Dr.-Ing. U. Nackenhorst (Institute of Mechanics and Computational Mechanics, Hanover University) for their contribution in the implementation of the mechanical model. We also thank PD Dr. rer. nat. M. Maischak (Institute of Applied Mathematics, Hanover University) for his contribution and valuable discussions on numerical coupling. This work has been supported by the German Research Foundation (DFG), GRK 615.

REFERENCES

1. Bhushan, B., *Handbook of Nano-technology*, Springer, Berlin, 2004.
2. Morita, S., R. Wiesendanger, and E. Meyer, *Noncontract Atomic Force Microscopy*, Springer, 2002.
3. Jacobs, H. O., P. Leuchtmann, O. J. Homan, and A. Stemmer, "Resolution and contrast in Kelvin probe force microscopy," *Journal of Applied Physics*, Vol. 84, No. 3, 1998.
4. Jackson, J. D., *Classical Electrodynamics*, Wiley, 1975.
5. Reddy, J. N., *Finite Element Method*, McGraw-Hill International Editions, Singapore, 1993.
6. Li, Z. C., *Numerical Methods for Elliptic Problems with Singularities*, World Scientific, 1990.
7. Costabel, M., "A symmetric method for the coupling of finite elements and boundary elements," *The Mathematics of Finite Elements and Applications*, Vol. 6, 281–288, 1988.
8. Stephan, E. P., "Coupling of boundary element methods and finite element methods," *Encyclopedia of Computational Mechanic*, Vol. 1, Chapter 13, 375–412, 2004.
9. Belytschko, T., W. K. Liu, and B. Moran, *Nonlinear Finite Elements for Continua and Structures*, Wiley, Sussex, 2004.

EM Field Induced in Inhomogeneous Dielectric Spheres by External Sources

G. C. Kokkorakis, J. G. Fikioris, and G. Fikioris
National Technical University of Athens, Greece

Abstract—The electromagnetic field induced in the interior of inhomogeneous dielectric bodies by external sources can be evaluated by solving the well-known electric field integrodifferential equation (EFIDE). For spheres with constant magnetic permeability μ, but variable dielectric constant $\varepsilon(r,\theta,\varphi)$ a direct, mainly analytical solution can be used even in case when the inhomogeneity in ε renders separation of variables inapplicable. This approach constitutes a generalization of the hybrid (analytical-numerical) scalar method developed by the authors in two recent papers, for the corresponding acoustic (scalar) field induced in spheres with variable density and/or compressibility. This extension, by no means trivial, owing to the vector and integrodifferential nature of the equation, is based on field-vector expansions using the set of three harmonic surface vectors, orthogonal and complete over the surface of the sphere, for their angular (θ,φ) dependence, and Dini's expansions of a general type for their radial functions. The use of the latter has been shown to be superior to other possible sets of orthogonal expansions and as far as its convergence is concerned it may further be improved by properly choosing a crucial parameter in their eigenvalue equation. The restriction to the spherical shape is imposed here to allow use of the well-known expansion of Green's dyadic in spherical eigenvectors of the vector wave equation.

1. Introduction

The motivation for solving volume integral equations in the case of penetrable (dielectric) spheres with varying dielectric constant $\varepsilon(\vec{r})$ (the magnetic permeability is considered constant throughout) have been discussed thoroughly in a previous paper by the authors [1], dealing with the corresponding scalar problem. The mathematical difficulties of various approaches have been treated in this paper [1], particularly in connection with the advantages of the direct hybrid method proposed here and in [1, 2] by the authors. A first generalization of the approach in acoustics concerned spheres with inhomogeneous density $\rho(\vec{r})$ [2] and herein a further generalization to the vector EM case is developed. In more specific terms we are concerned with the well-known electric field integrodifferential equation (EFIDE)

$$\vec{E}(\vec{r}) = \vec{E}^i(\vec{r}) + \frac{1}{4\pi}(k_0^2 + \nabla\nabla\bullet)\iiint_V (\frac{\varepsilon(\vec{r}')}{\varepsilon_0} - 1)\vec{E}(\vec{r}')\frac{e^{-ik_0R}}{R}dV' \tag{1}$$

via which the EM field $\vec{E}(\vec{r})$, induced in the interior of an inhomogeneous dielectric body of volume V with varying dielectric constant $\varepsilon(\vec{r})$ (ε_0 is its free space value, while the magnetic permeability μ_0 is considered constant throughout), is evaluated [3–5]. In (1) $\vec{E}^i(\vec{r})$ is the imposed incident field, $R = |\vec{r} - \vec{r}'|$, $k_0 = \omega\sqrt{\mu_0\varepsilon_0} = 2\pi/\lambda$, while $\exp(i\omega t)$ is the assumed time dependence. The induced interior field in V is of primary importance to questions of radiation hazards, to the setting of reliable safety field strength limits in media like living tissue, human heads exposed to nearby EM sources, etc. Following the evaluation of the induced interior field the exterior, scattered one may also be obtained by direct integration.

If V is restricted to be a sphere of radius "a", even when the inhomogeneity $\varepsilon(\vec{r})$ precludes separation of variables, a virtually analytical method can be used to solve (1) based on the possibility of expanding the free space Green's function $G(R) = e^{-ik_0R}/4\pi R$ into an infinite series of spherical eigenfunctions of the Helmholtz equation [1, 2]. This well-known expansion, shown here in the following equation (2) for the corresponding Green's dyadic, is available only in spherical coordinates and combined with Dini-type expansions for the radial functions of the field vectors, provides a basis for a virtually analytical approach. The expansion of Green's dyadic in spherical coordinates is given on page 1875 of [8] in terms of the even/odd spherical eigenvectors of the vector Helmholtz equation. Here we use a more convenient form in terms of the complex form of these vectors as in [9]

$$\begin{aligned}\bar{\bar{G}}(\vec{r},\vec{r}) \;=\; \bar{\bar{I}}\frac{e^{-ik_0|\vec{r}-\vec{r}'|}}{|\vec{r}-\vec{r}'|} = -\frac{ik_0}{4\pi}\sum_{n=1}^{\infty}\frac{2n+1}{n(n+1)}\sum_{m=-n}^{n}\frac{(n-m)!}{(n+m)!}[\vec{M}^{(1)}_{mn}(k_0,r_<,\theta,\varphi)\widehat{\vec{M}}^{(4)}_{mn}(k_0,r_>,\theta',\varphi') \\ +\vec{N}^{(1)}_{mn}(k_0,r_<,\theta,\varphi)\widehat{\vec{N}}^{(4)}_{mn}(k_0,r_>,\theta',\varphi') + n(n+1)\vec{L}^{(1)}_{mn}(k_0,r_<,\theta,\varphi)\widehat{\vec{L}}^{(4)}_{mn}(k_0,r,\theta',\varphi')]\end{aligned} \tag{2}$$

This form can easily be shown to be equivalent to that of [8, 9], where the definitions of the various symbols used here can be found.

2. Solution of the EFIDE

To solve the EFIDE we expand the unknown electric field in vector wave functions in the interval [0, a] in a manner analogous to that of Chew for unbounded media [9, p.397]. The calculation is facilitated by taking into account Gauss's law $\nabla \cdot \vec{D} = 0$, which leads us to write

$$\frac{\varepsilon(\vec{r})}{\varepsilon_0}\vec{E}(\vec{r}) = \sum_{n=1}^{\infty}\sum_{m=-n}^{n}\sum_{l=1}^{\infty}\left[A_{mn\ell}\vec{M}_{mn\ell}(\frac{\gamma^M_{mn\ell}}{a},\vec{r}) + B_{mn\ell}\vec{N}_{mn\ell}(\frac{\gamma^N_{mn\ell}}{a},\vec{r})\right] \tag{3}$$

excluding the vector $\vec{L}$ from the expansion. Similarly we expand the incident field. Here, we have restricted the spectrum of the values of k in the definitions of the vectors $\vec{M}_{mn}(k, \vec{r})$etc, to discrete sets of values $\gamma^M_{mn\ell}$, $\gamma^N_{mn\ell}$, $\ell = 1, 2, ...$, which have been chosen so as to construct a full orthogonal set of vectors $\vec{M}$ and $\vec{N}$, respectively, over the volume of the sphere $0 \le r \le a$, $0 \le \theta \le \pi$, $0 \le \varphi \le 2\pi$. Moreover, all vectors $\vec{M}_{mn\ell}$ and $\vec{N}_{mn\ell}$ in those orthogonal relations are vectors of the first kind, i. e., $\vec{M}_{mn\ell} = \vec{M}^{(1)}_{mn\ell}$, with the upperscript (1) deleted throughout. We can then make use of results like

$$\begin{aligned} I(\vec{M}_{mn\ell}, \hat{\vec{M}}_{\mu vp}) &= \int_0^a\int_0^\pi\int_0^{2\pi}\vec{M}_{mn\ell}(\frac{\gamma^M_{mn\ell}}{a},\vec{r})\cdot\hat{\vec{M}}_{\mu vp}(\frac{\gamma^M_{\mu vp}}{a},\vec{r})r^2\sin\theta dr d\theta r d = 4\pi\frac{n(n+1)}{2n+1}\frac{(n+m)!}{(n-m)!} \\ &\delta_{m\mu}\delta_{nv}\frac{a^3 j_n(\gamma^M_{mn\ell})j_n(\gamma^M_{mnp})}{(\gamma^M_{mn\ell})^2-(\gamma^M_{mnp})^2}\left[\frac{\gamma^M_{mn\ell}j'_n(\gamma^M_{mn\ell})}{j_n(\gamma^M_{mn\ell})}-\frac{\gamma^M_{mnp}j'_n(\gamma^M_{mnp})}{j_n(\gamma^M_{mnp})}\right], l \ne p \end{aligned} \tag{4}$$

and similar ones for the $\overrightarrow{N}$ and $\overrightarrow{L}$ vectors. Analogous relations for the scalar case were found in [1, 2]. We can now establish full orthogonality of the set over the volume of the sphere by selecting $\gamma^M_{mn\ell}$ as the roots of the "M-eigenvalue equation"

$$\frac{\gamma^M_{mn\ell}j'_n(\gamma^M_{mn\ell})}{j_n(\gamma^M_{mn\ell})} \equiv t^M_{mn}(\ell = 1, 2, \ldots) \tag{5}$$

in which t^M_{nm} may be any chosen constant. Orthogonality of the N-set over the volume of the sphere is, also, established if we choose $\gamma^N_{mn\ell}$ as the roots of the "N-eigenvalue equation"

$$\frac{[\gamma^N_{mn\ell}j_n(\gamma^N_{mn\ell})]'}{(\gamma^N_{mn\ell})^2 j_n(\gamma^N_{mn\ell})} \equiv t^N_{nm}(\ell = 1, 2, \ldots) \tag{6}$$

Finally for the L-set the corresponding $\gamma^L_{mn\ell}$ are chosen as the roots of the "L-eigenvalue equation"

$$\frac{j'_n(\gamma^L_{mn\ell})}{\gamma^L_{mn\ell}j_n(\gamma^L_{mn\ell})} \equiv t^L_{nm}(l = 1, 2, \ldots) \tag{7}$$

Last, but not least, we must establish the orthogonality between the $\vec{L}_{\mu\nu p}$ and $\vec{N}_{mn\ell}$ sets, which is not assured from their angular part (θ, φ) only. However, over the volume of the sphere we have

$$\begin{aligned} I(\vec{N}_{mn\ell}, \hat{\vec{L}}_{\mu vp}) &= \int_V dV'\vec{N}_{mn\ell}(k^N_\ell, \vec{r})\cdot\hat{\vec{L}}_{\mu vp}(k^L_p, \vec{r}) \\ &= 4\pi\frac{n(n+1)}{2n+1}\frac{(n+m)!}{(n-m)!}\delta_{m\mu}\delta_{nv}\frac{a^3}{\gamma^N_{mn\ell}\gamma^L_{mnp}}j_n(\gamma^N_{mn\ell})j_n(\gamma^L_{mnp}) \end{aligned} \tag{8}$$

and orthogonality is assured if we choose the roots of $j_n(\gamma^L_{mnp}) = 0$ for the $\vec{L}$ vectors.
We write also

$$\vec{E}(\vec{r}) = \sum_{n=1}^{\infty}\sum_{m=-n}^{n}\sum_{l=1}^{\infty}\left[\Gamma_{mn\ell}\vec{M}_{mn\ell}(\frac{\gamma^M_{mn\ell}}{a},\vec{r}) + \Delta_{mnl}\vec{N}_{mn\ell}(\frac{\gamma^N_{mn\ell}}{a},\vec{r}) + Z_{mn\ell}\vec{L}_{mn\ell}(\frac{\gamma^L_{mn\ell}}{a},\vec{r})\right] \tag{9}$$

The calculation is carried out with the help of the following intermediate results

$$\begin{aligned} I(\vec{M}\cdot\bar{\bar{I}}g) &= \int_V dV'\vec{M}_{mn\ell}(k,\vec{r}')\cdot\bar{\bar{I}}g(\vec{r},\vec{r}') = \frac{1}{k^2-k_0^2}\{\vec{M}_{mn\ell}(k,\vec{r}) - ik_0a^2[-kj'_n(ka)h_n(k_0a) \\ &+k_0h'_n(k_0a)j_n(ka)]\vec{M}_{mn}(k_0,\vec{r})\} \end{aligned} \tag{10}$$

$$I(\vec{N}\cdot\bar{\bar{I}}g) = \int_V dV'\vec{N}_{mn\ell}(k,\vec{r}')\cdot\bar{\bar{I}}g(\vec{r},\vec{r}') = \frac{1}{k^2-k_0^2}\{\vec{N}_{mn\ell}(k,\vec{r}) - ik_0a^2[kj_n(ka)\frac{1}{k_0a}\left[xh_n(x)\right]'_{x=k_0a}$$
$$-k_0h_n(k_0a)\frac{1}{ka}\left[xj_n(x)\right]'_{x=ka}]\vec{N}_{mn}(k_0,\vec{r})\} - ik_0a^2n(n+1)\frac{j_n(ka)h_n(k_0a)}{akk_0}\vec{L}_{mn}(k_0,\vec{r}) \quad (11)$$

$$I(\vec{L}\cdot\bar{\bar{I}}g) = \int_V dV'\vec{L}_{mn\ell}(k,\vec{r}')\cdot\bar{\bar{I}}g(\vec{r},\vec{r}') = \frac{1}{k^2-k_0^2}\{\vec{L}_{mn\ell}(k,\vec{r}) - ik_0a^2[kj_n(ka)h'_n(k_0a)$$
$$-k_0h_n(k_0a)j'_n(ka)]\vec{L}_{mn}(k_0,\vec{r})\} - ik_0a^2\frac{j_n(ka)h_n(k_0a)}{akk_0}\vec{N}_{mn}(k_0,\vec{r}) \quad (12)$$

In all the above equations $k=\frac{\gamma^X_{mnl}}{a}$, with $X=M$ or N or L respectively.

After lengthy manipulations we get the system of equations

$$\Gamma_{mn\ell} = A^{inc}_{mn}T^M_{n\ell}(k_0) + k_0^2\frac{A_{mn\ell}-\Gamma_{mn\ell}}{\left(\frac{\gamma^M_{mn\ell}}{a}\right)^2-k_0^2}$$
$$-ik_0^3a^2T^M_{n\ell}(k_0)\sum_{\mathrm{p}}\frac{\left[-\frac{\gamma^M_{mnp}}{a}j'_n(\gamma^M_{mnp})h_n(k_0a)+k_0h'_n(k_0a)j_n(\gamma^M_{mnp})\right]}{\left(\frac{\gamma^M_{mnp}}{a}\right)^2-k_0^2}(A_{mnp}-\Gamma_{mnp}) \quad (13)$$

$$\Delta_{mn\ell} = B^{inc}_{mn}T^N_{n\ell}(k_0) + k_0^2\frac{B_{mn\ell}-\Delta_{mn\ell}}{\left(\frac{\gamma^N_{mn\ell}}{a}\right)^2-k_0^2} - ik_0^3a^2T^N_{n\ell}(k_0)\cdot$$
$$\sum_p\frac{\left[\frac{\gamma^N_{mnp}}{a}j_n(\gamma^N_{mnp})\frac{1}{k_0a}\left[xh_n(x)\right]'_{x=k_0a} - k_0h_n(k_0a)\frac{1}{\gamma^N_{mnp}}\left[xj_n(x)\right]'_{x=ka}\right]}{\left(\frac{\gamma^N_{mnp}}{a}\right)^2-k_0^2}(B_{mnp}-\Delta_{mnp}) \quad (14)$$

where $T^M_{n\ell}(k_0)$ and $T^N_{n\ell}(k_0)$ are obviously the expansions coefficients of $\vec{M}_{mn}(k_0,\vec{r})$, $\vec{N}_{mn}(k_0,\vec{r})$ over the orthogonal sets $\vec{M}_{mn\ell}$ and $\vec{N}_{mn\ell}$, $\ell=1,2,...,$ respectively.

The next step is to eliminate one of the two groups of unknowns $\{\mathrm{A},\mathrm{B}\}$ or $\{\Gamma,\Delta,\mathrm{Z}\}$. Since Z are not present in the final expressions it is better to eliminate Γ,Δ, so we write

$$\vec{E} = \frac{1}{\frac{\varepsilon(\vec{r})}{\varepsilon_0}}\sum_{m,n,\ell}\left[A_{mn\ell}\vec{M}_{mn\ell}+B_{mn\ell}\vec{N}_{mn\ell}\right] = \sum_{m,n,\ell}\left[\Gamma_{mn\ell}\vec{M}_{mn\ell}+\Delta_{mn\ell}\vec{N}_{mn\ell}+Z_{mn\ell}\vec{L}_{mn\ell}\right] \quad (15)$$

We have thus constructed the necessary equations which, via the orthogonality relations, lead to a matrix equation for the unknowns A, B.

3. Numberical Results and Discussion

Numerical results were obtained for both radial and r-,θ- dependence of the inhomogeneities. For the simpler r-case we selected the well known case of Eaton lens, $\varepsilon(r)=(r/a)^2$ [11, 12]. We have then reproduced exactly the same results known from the literature.

We next present results for the more complicated $r-$, $\theta-$ case. Here we have worked without optimizing the t_{mn} values (a complicated problem) and without comparison to existing results, that are lacking in this more general case. However, a confirmation of the correctness of our procedure stems from the reproduction of our results with other random choices for t_{mn}.

For convenience, that is to obtain as many intermediate results as possible in analytic form and reduce the numerical burden, we have chosen the following function

$$\varepsilon(\vec{r}) = \frac{\varepsilon_0}{1+0.3\left(\frac{r}{a}\right)^2\cos\theta} \quad (16)$$

Here, working with $k_0a=2.0958$ and using as incident field a plane wave $\hat{x}e^{ikz}$ [10], we present final results for the total interior field $|\vec{E}^{tot}(r,\,\theta,\,\varphi=0)/E_0|$($E_0$ is the amplitude of $\vec{E}_{inc}$) for a few particular values of θ, which

is treated as a parameter in the Figure. Our results correspond to $\varphi = 0$. It turned out that we should take $n = 5$ terms for the M-component and $n = 10$ terms for the N-component. In all cases we used $\ell_T = 12$ terms and this proved to be sufficient.

The maximum value of the total interior field appears at $r/a = 0.95$ and $\theta = 77°$.

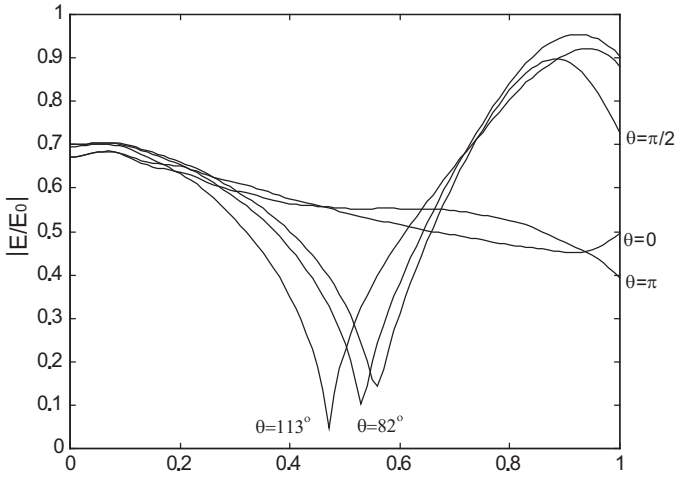

Figure 1: $|E|$ for $\varepsilon(\vec{r}) = \varepsilon_0 \left(1 + 0.3 \left(\frac{r}{a}\right)^2 \cos\theta\right)^{-1}$, $k_0 a = 2.0958$ for various θ, incident field $\hat{x}e^{ikz}$.

Acknowledgement

The present work has been supported by the Empirikion Foundation of Greece.

REFERENCES

1. Kokkorakis, G. C., J. G. Fikioris, and G. Fikioris, "Field induced in inhomogeneous spheres by external sources.I. The scalar case," *J. Acoust. Soc. Am.*, Vol. 112, No. 4, 1297–1306, October 2002.
2. Kokkorakis, G. C. and J. G. Fikioris, "Acoustic field induced in spheres with inhomogeneous density by external sources.," *J. Acoust. Soc. Am.*, Vol. 115, No. 2, 478–487, Feburary 2004.
3. Van Bladel, J., *Electromagnetic Fields*, Mc Graw–Hill Book Co., Inc., New York, 1964.
4. Fikioris, J. G., "Electromagnetic field of in the source region of continuously varying current density," *Quart. Appl. Math.*, Vol. LIV, No. 2, 201–209, June 1996.
5. Fikioris, J. G., "The EM field of constant current density distributions in parallelepiped regions," *IEEE Trans. Antennas Propagat.*, Vol. 46, No. 9, 1358–1364, Septemper 1998.
6. Fikioris, J. G., "On the singular integrals in the source region of electromagnetic fields," *J. Electromagnet. Wave and Appl.*, Vol. 18, No. 10, 1505–1521, November 2004.
7. Fikioris, J. G. and A. N. Magoulas, "Scattering from axisymmetric scatterers: A hybrid method of solving Maue's equation," *Progress in Electromagnetics Research*, PIER 25, 131–165, 2000.
8. Morse, P. M. and H. Feshbach, *Methods of Theoretical Physics*, McGraw–Hill Book Co., New York, 1953.
9. Chew, W. C., *Waves and Fields in Inhomogeneous Media*, Van Nostrand Reinhold, New York, 1990.
10. Stratton, J. A., *Electromagnetic Theory*, New York, 1941.
11. Tai, C. T., *Dyadic Green's Functions in Electromagnetic Theory*, Intext Educational Publihers, 1971.
12. Rozenfeld, P., "The electromagnetic theory of three-dimensional inhomogeneous lenses," *IEEE Trans. Antennas Propagat.*, Vol. 24, 365–370, May 1976.

Spatial-spectral Hybrid Method in Calculation of Capacitances and Inductances of Ring Conductors in a Stratified Medium

T. J. Dufva
Helsinki University of Technology, Finland

J. C.-E. Sten
VTT Technical Research Centre of Finland, Finland

In addition to generic numerical integration equation methods in electromagnetics, there is also a need for simplier algorithms for some basic geometries. These algorithms may be used as efficient and accurate models for some RF-components, for example, or they may served as benchmarks for more generic algorithms. An example of such algorithms is the one presented earlier by the authors [1]. The paper treats the calculation of the capacitances and inductances of the system of thin ring conductors in a stratified medium. These parameters were found by solving the surface charge and current distributions on the rings by using Galerkin method and the spectral method. The present work generalises the above algorithm for thick ring conductors.

The spectral method utilising an integral transform in the transverse plane is commonly used in the analysis of planar structures in a stratified medium. This is because the solution of the Green's function is more straightforward in the spectral domain. However, if the coupling integrals between the basis functions are to be evaluated in the spatial domain, the tedious inverse transform of the spectral Green's function must be carried out for every integration point. Another solution is to calculate the coupling integrals in the spectral domain. Unfortunately, the infinity integrals which arise are also laborious due to the highly oscillating and slowly decaying integrands. The so-called spatial-spectral hybrid method exploits the benefits of the pure spectral method but avoids the most troublesome integrals. In the method the Green's function and the coupling integrals are divided into two parts. The first part of the Green's function includes the primary point source and the first reflections from the interfaces of the medium, found from the image theory. The corresponding parts of the coupling integrals are evaluated in the spatial domain. The rest of the Green's function and the corresponding parts of the coupling integrals are calculated in the spectral domain. Although the integrands are oscillating like in the pure spectral method, they decay exponentially because the asymptotic part of the spectral Green's function is contained in the first part evaluated in the spatial domain.

The unknown surface charge and current distributions on the faces of the conducting rings are estimated as superpositions of entire-domain basis functions. Each of the basis functions includes the correct edge behaviour and together they constitute a complete and quickly converging expansion for the distributions. The integral transforms of the basis functions needed in the method are found in analytic form.

REFERENCES

1. Dufva, T. J., and J. C.-E. Sten, "Quasi-static variational analysis of planar spiral conductors," *Journal of Electromagnetic Waves and Applications*, Vol. 16, No. 7, 957–976, 2002.